frontiers in Energy Research

ORIGINAL RESEARCH
published: 18 March 2022
doi: 10.3389/fenrg.2022.865856

Simulation Study on Lightning Impulse Characteristics of Flexible Graphite Composite Grounding Materials Applied to Grounding Grid of Power System

Yuanchao Hu[1], Tao Huang[2], Yunzhu An[1], Jianyuan Feng[1], Meng Cheng[2], Hongping Xie[2], Wentao Shen[2] and Changqing Du[2]*

[1]School of Electrical and Electronic Engineering, Shandong University of Technology, Zibo, China, [2]Construction Branch of State Grid Jiangsu Electric Power Co., Ltd, Nanjing, China

The flexible graphite composite grounding electrode is a non-metallic grounding electrode with good electrical conductivity, corrosion resistance and non-ferromagnetic properties. In order to analyze the impulse characteristics of the graphite composite grounding electrode, this paper builds a frequency domain electrical network model and an equivalent radius iterative algorithm, considering skin effect, inductance effect, capacitance effect and spark discharge effect. The impulse characteristics of typical metal grounding electrodes and graphite composite grounding electrodes are analyzed by simulation. The research results show that: Compared with the traditional metal grounding electrode, the graphite composite grounding electrode has a smaller skin and inductance effect under the action of the impulse current, and a better current flowing capability; as the soil resistivity increases, the inductance effect and the skin effect are weakened, while the spark discharge effect is gradually enhanced and dominates. The spark discharge effect can effectively decrease the grounding resistance. The obtained critical value of the normalized parameter of 412 kA Ω, can be taken as the threshold to discriminate the conditions with dominate inductance effect from the conditions with dominant spark discharge effect.

Keywords: power system grounding electrode, graphite composite grounding electrode, impulse characteristics, spark discharge effect, inductance effect, electrical network model

OPEN ACCESS

Edited by:
Xun Shen,
Tokyo Institute of Technology, Japan

Reviewed by:
Hardeep Singh,
Sophia University, Japan
Vikram Kamboj,
Lovely Professional University, India

****Correspondence:***
Yunzhu An
anyunzhu2006@163.com

Specialty section:
This article was submitted to Smart Grids, a section of the journal Frontiers in Energy Research

Received: *30 January 2022*
Accepted: *21 February 2022*
Published: *18 March 2022*

Citation:
Hu Y, Huang T, An Y, Feng J, Cheng M, Xie H, Shen W and Du C (2022) Simulation Study on Lightning Impulse Characteristics of Flexible Graphite Composite Grounding Materials Applied to Grounding Grid of Power System. Front. Energy Res. 10:865856. doi: 10.3389/fenrg.2022.865856

INTRODUCTION

The grounding grid is the most basic lightning protection device in power system. Good impulse grounding performance is an important prerequisite for ensuring safe and reliable operation of power system. The grounding resistance of grounding device generated by lightning current is called impulse grounding impedance (Deng et al., 2013; He and Zhang, 2015; Zhang, 2018). Different from the power frequency current, the lightning current flows through the grounding electrode in a pulse manner in a very short time, resulting in that the impulse grounding impedance is different from the power frequency grounding resistance (Grcev, 2009a) (Tao et al., 2018). The lightning current flowing through grounding electrode and soil is a complex electromagnetic transient process accompanied by various physical effects such as inductance effect and spark discharge effect (Grcev, 2009b; Visacro and Rosado, 2009; Deng et al., 2012; Wen et al., 2016). The CDEGS, an international general grounding simulation software, can be used

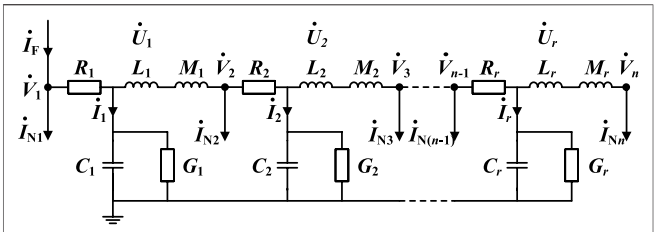

FIGURE 1 | Equivalent electrical network model of grounding electrode.

to calculate the impulse grounding impedance of grounding electrode. However, the calculation results of CDEGS do not consider the influence of soil ionization, which is called spark discharge effect in this paper, leading to a large error between the calculation results and the actual grounding impedance of the grounding electrode (Yang et al., 2021; Feng et al., 2015). At present, the numerical simulation algorithms for impulse characteristics of grounding devices considering the effect of soil spark discharge mainly include transmission line modeling method (TLM) and finite element method (FEM). The impulse response of grounding devices using TLM is equivalent to the wave propagation of transmission line. This method cannot consider the coupling between conductors (de Lima and Portela, 2007; Gazzana et al., 2014). The FEM method is more efficient, but the change of soil resistivity will lead to the occurrence of ill-conditioned matrix in the calculation, thus affecting the calculation accuracy (Nekhoul et al., 1996). It is difficult to consider all the physical processes like skin effect, inductance effect and spark discharge process when impulse current flew through the grounding electrode.

In recent years, flexible graphite composite grounding material as a new type of non-magnetic grounding electrode has been applied to the grounding grids of power system (Huang et al., 2019; Hu et al., 2014). Compared with traditional metal grounding materials, flexible graphite composite grounding materials have good electrical conductivity and natural corrosion resistance (Gong et al., 2016; Hu et al., 2016; Xiao et al., 2017). In order to study the impulse characteristics of graphite composite grounding electrode under the influence of skin effect, inductance effect and capacitance effect, the frequency domain electrical network model is established by MATLAB to simulate the current flow process of tower grounding electrode. Moreover, the iterative algorithm of equivalent radius is used to consider the influence of soil nonlinear ionization around the grounding electrode. The influences of various physical effects on the impulse characteristics of graphite composite grounding electrode are obtained by simulation. The research results can provide theoretical reference for optimizing the length of graphite composite grounding electrode.

SIMULATION MODELING METHOD

Frequency Domain Electrical Network Model of Grounding Electrode

In this section, the impulse process of grounding electrode in Earth is considered by frequency domain electrical network model. A simple horizontal grounding electrode is applied. In order to describe the grounding electrode more intuitively, this paper adopts the circuit modeling with lumped parameters. Firstly, the grounding electrode is gridded and each segment is equivalent to a circuit model composed of resistance, inductance, grounding capacitance and grounding conductance (Mentre and Grcev, 1994) (Lorentzou et al., 2003). The equivalent electrical network model of horizontal grounding rod is shown in **Figure 1**.

Suppose there are a total of r branches, n nodes, so that the branches $i = 1, 2, \cdots, r$, nodes $j = 1, 2, \cdots, n$, where R_i, L_i, M_i, C_i and G_i are the resistance, self-inductance, mutual-inductance, grounding capacitance, and grounding conductance of each branch after the grounding electrode meshing; $\dot{U}_i$ and $\dot{V}_j$ are the ground potential rises (GPR) of each segment of branch and each node relative to infinity; $\dot{I}_F$ is the external injection impulse current; $\dot{I}_i$ and $\dot{I}_{Nj}$ are the currents flowing into the Earth for each branch and each node.

Assuming that the GPR of each segment of the branch is equal to the average value of the GPR at both ends, as shown in **Eq. 1**.

$$\dot{\boldsymbol{U}}_i = \frac{\dot{\boldsymbol{V}}_i + \dot{\boldsymbol{V}}_{i+1}}{\mathbf{2}} \tag{1}$$

According to **Eq. 1**, the matrix relation between GPR vector $\dot{\mathrm{U}}$ of branch and GPR vector $\dot{\mathrm{V}}$ of node can be obtained.

$$\dot{\boldsymbol{U}} = \boldsymbol{K}\dot{\boldsymbol{V}} \tag{2}$$

where $\boldsymbol{K}$ is the relationship matrix between the branch and the node. When branch i is associated with node j, the corresponding value is 0.5, otherwise the value is 0.

Assuming that the current distribution on each branch is uniform, and the current at each node is equal to the average value of the branch current connected to it. Similarly, the vector relation of the current flowing into the Earth on nodes and branches can be obtained, as shown in **Eq. 3**.

$$\dot{\boldsymbol{I}}_{\mathbf{N}} = \boldsymbol{K}^{\boldsymbol{T}}\dot{\boldsymbol{I}} \tag{3}$$

where $\boldsymbol{K}^{\mathrm{T}}$ is the transposed matrix of $\boldsymbol{K}$.

The vector $\dot{I}$ of branch current flowing into the Earth and the vector $\dot{U}$ of branch GPR have the constraint relationship of **Eq. 4**.

$$\dot{\boldsymbol{U}} = \boldsymbol{Z}\dot{\boldsymbol{I}} \tag{4}$$

where $\boldsymbol{Z}$ is the impedance matrix of conductor grounding branch. The elements in $\boldsymbol{Z}$ are composed of the self-impedance of each branch and the mutual impedance between branches.

Inverse matrix $\boldsymbol{Z}$ and get **Eq. 5**.

$$\dot{\boldsymbol{I}} = \boldsymbol{Y}_{\mathbf{B}}\dot{\boldsymbol{U}} \tag{5}$$

According to the node voltage equation, **Eq. 6** is obtained.

$$\dot{\boldsymbol{I}}_{\mathbf{F}} - \dot{\boldsymbol{I}}_{\mathbf{N}} = \boldsymbol{Y}_{\mathbf{N}}\dot{\boldsymbol{V}} \tag{6}$$

where Y_N is the node admittance matrix composed of the resistance and inductance of each branch.

Eq. 7 can be obtained by **Eqs 2**, **3**, **5**, and **6**.

$$\dot{\boldsymbol{I}}_{\mathbf{F}} = \left(\boldsymbol{K}^{\mathrm{T}}\boldsymbol{Y}_{\mathbf{B}}\boldsymbol{K} + \boldsymbol{Y}_{\mathbf{N}}\right)\dot{\boldsymbol{V}} \tag{7}$$

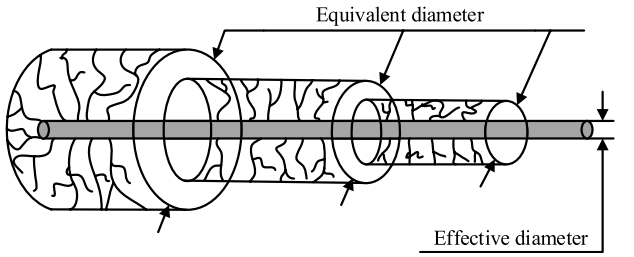

FIGURE 2 | Physical model of spark discharge field of soil around grounding electrode.

According to **Eq. 7**, the vector $\dot{V}$ of node GPR can be obtained, and the vector $\dot{U}$ of branch GPR and the vector $\dot{I}$ of branch current flowing into the Earth are obtained by **Eqs 2**, **5**.

It is required to solve the impulse response curve of grounding electrode in the time domain. Firstly, the pulse current in the time domain is decomposed into a plurality of sinusoidal alternating currents with different frequencies by fast Fourier transform (FFT). Under the action of current with different frequencies, the corresponding branch admittance matrix Y_B and node admittance matrix Y_N can be solved, thereby obtaining vector values of voltage and current. Finally, the frequency domain response is transformed into the corresponding time domain response through the inverse Fourier transform, and the impulse response curve of parameters such as branch GPR and current flowing into Earth can be obtained.

Iterative Algorithm Considering Spark Discharge Effect

In order to consider the influence of spark discharge effect on the impulse characteristics of grounding electrode, it is assumed that the spark discharge area generated around each branch of the grounding electrode is a cylinder with uniform ionization. The equivalent model of grounding electrode during discharge is shown in **Figure 2** (Shen and Raksincharoensak, 2021a; Shen and Raksincharoensak, 2021b).

Under the influence of sinusoidal alternating current at different frequencies, the grounding electrode surface and the surrounding soil will produce different electric field intensities $E_i(\omega)$ and current densities $J_i(\omega)$, as shown in **Eq. 8**.

$$\boldsymbol{J_i(\omega) = \frac{E_i(\omega)}{\rho} + j\omega\varepsilon E_i(\omega)} \tag{8}$$

where ρ is the soil resistivity; ω is the angular frequency of the sinusoidal alternating current; ε is the dielectric constant of the soil.

The current density of the grounding electrode surface can be determined by the branch current flowing into the Earth. According to **Eq. 8**, the relationship between the electric field intensity $E_i(\omega)$ and the equivalent radius r of spark discharge can be obtained as shown in **Eq. 9** (Shen et al., 2022).

$$\boldsymbol{E_i(\omega) = \frac{I_i(\omega)}{2\pi r l\left(1/\rho + j\omega\varepsilon\right)}} \tag{9}$$

The instantaneous value of electric field intensity in time domain is calculated by inverse Fourier transform of soil electric field intensity $E_i(\omega)$ around grounding electrode in frequency domain. By simplifying, the relationship between the equivalent radius $r_i(t)$ of the grounding electrode spark discharge and its surrounding soil electric field intensity $E_i(t)$ in the time domain is shown in **Eq. 10**.

$$\boldsymbol{\frac{r_i(t)}{r} = \frac{E_i(t)}{E_C}} \tag{10}$$

where $r_i(t)$ is the equivalent radius of the branch i; r is the real radius of the grounding electrode; E_c is the critical breakdown field strength of soil. If $E_i(t) > E_c$, the soil around the grounding electrode is broken down, resulting in spark discharge. The equivalent radius of the branch is calculated by **Eq. 10**. If $E_i(t) \le E_c$, it is calculated according to the real radius r.

With the change of equivalent radius $r_i(t)$, the self-admittance parameter in the grounding branch admittance matrix Y_B changes, thereby affecting the change of branch current flowing into the Earth. At the same time, the flowing current will change the value of the equivalent radius. The two interact, and the change of its value is an iterative process. The simulation calculation process is shown in **Figure 3**. The $k(t)$ is the ratio of the estimated branch GPR vector $\dot{U}$, which can be solved by the constraint condition that the sum of the currents $\dot{I}$ flowing into the Earth at each moment is equal to the sum of the node impulse currents $\dot{I}_F$. The e is the convergence criterion of the iterative algorithm, namely the difference $\Delta r_{i\max}(t)$ of the maximum radius between the equivalent radius $r_i(t)$ mth

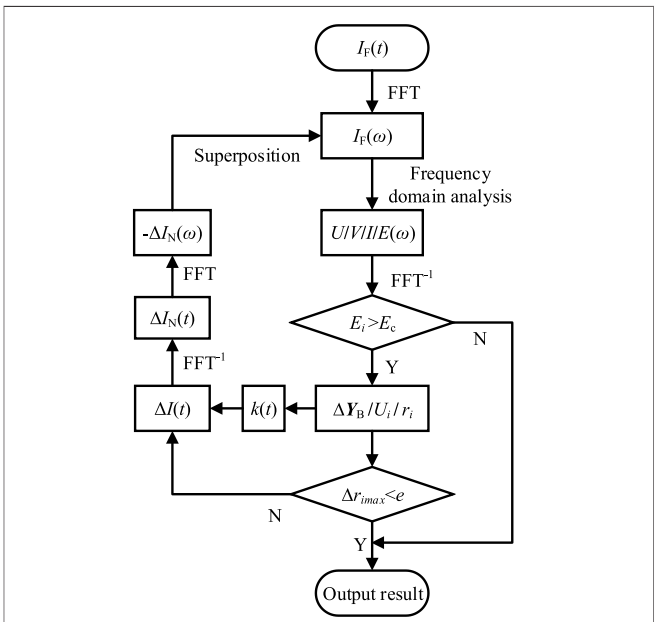

FIGURE 3 | Equivalent radius iterative algorithm flow chart.

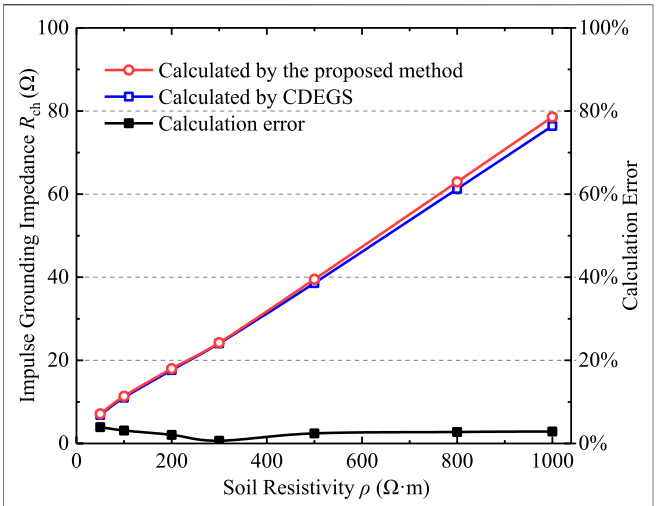

FIGURE 4 | Impulse grounding impedance curve without considering spark discharge effect.

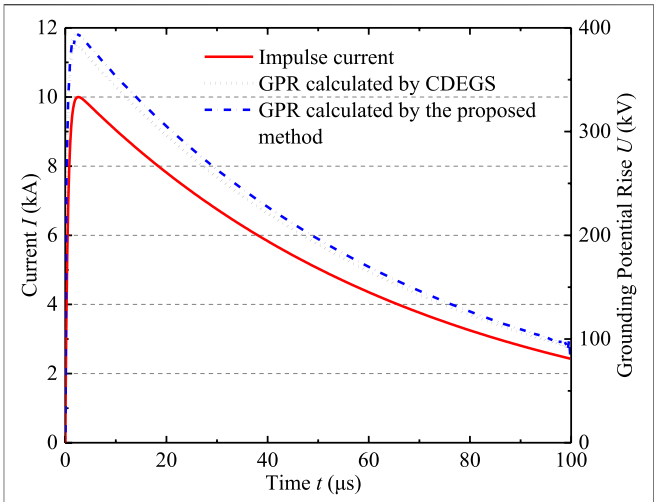

FIGURE 5 | Voltage response curve of grounding electrode when ρ is 500 Ω m.

iteration and the (m-1)th iteration. If the equivalent radius converges, the calculation result is directly output. Otherwise, the branch current variation $\Delta I_i(t)$ and node current variation $\Delta I_{Nj}(t)$ are obtained by the equivalent radius. The frequency domain value $\Delta I_{Nj}(\omega)$ is obtained by Fourier transform and superimposed into the reduction of external impulse current on the impulse current of the previous iteration. The simulation is continuously iteratively calculated until the equivalent radius converges.

VERIFICATION OF SIMULATION RESULTS

In order to verify the effectiveness of the frequency domain electrical network model and its iterative algorithm simulation results, the calculation results of this paper are compared with the calculation results of CDEGS grounding simulation software and the experimental results in the literature. Both simulations and experiments adopt round steel grounding electrodes. The grounding electrode radius is 10 mm, the length of grounding electrode is 20 m, the buried depth is 0.8 m, the impulse current waveform is 2.6/50 μs, the amplitude is 10 kA, the relative dielectric constant of sold is 9, and the soil critical breakdown field strength E_c is 400 kV/m (Mousa, 1994).

Without considering the effect of spark discharge, the variation curve of impulse grounding impedance R_{ch} of grounding electrode under different soil resistivities is obtained by frequency domain electrical network model simulation. The calculation results are compared with the simulation results of CDEGS, as shown in **Figure 4**.

The simulation results in this paper are basically consistent with the laws of CDEGS calculations, and the maximum error is less than 4%. **Figure 5** shows the time-domain voltage response curve of the grounding electrode when the soil resistivity ρ is 500 Ω m. It can be seen that the proposed method has good consistency with the calculation results of CDEGS, indicating that the calculation method of frequency domain electrical network model proposed in this paper is correct.

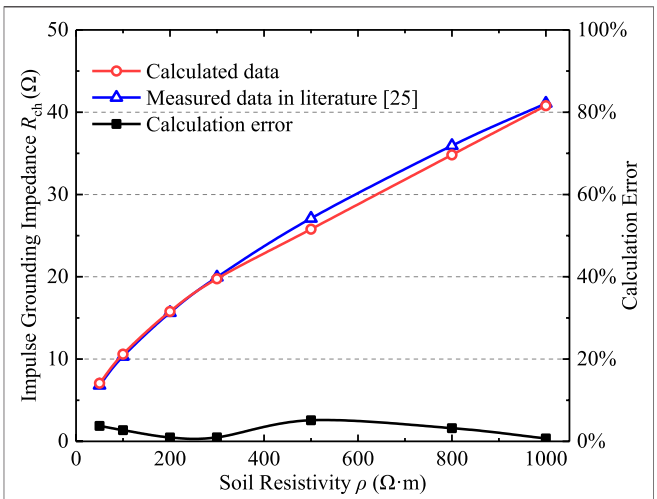

FIGURE 6 | Impulse grounding impedance curve considering spark discharge effect.

Moreover, this paper uses the equivalent radius iterative algorithm to simulate the soil discharge process, and compares its calculation results with the simulation results in literature (He et al., 2003), as shown in **Figure 6**. Affected by different soil resistivity, the impulse grounding impedance calculated by the equivalent radius iterative algorithm proposed in this paper is similar to the simulation experiment in literature (He et al., 2003), and the maximum error is less than 6%.

The calculated results of 20 m horizontal grounding electrode in soil with resistivity of 1,000 Ω m are compared with the results obtained from the full-scale experiments by Wen *et al* (Yang et al., 2022) in **Table 1**, where α is the impulse

TABLE 1 | Comparison with the impulse coefficient α of the experiment.

Impulse current	2 kA	4 kA	6 kA	8 kA
He et al. (2003)	0.63	0.59	0.57	0.55
Wen *et al.* (Yang et al., 2022)	0.68	0.59	0.55	0.52
calculated data	0.72	0.62	0.56	0.52

TABLE 2 | Material parameters of the steel and graphite grounding electrode.

Material	Diameter Φ(mm)	Resistivity δ(Ω·m)	Relative permeability ε_r
Steel	12	1.92×10^{-6}	636
Graphite	28	3.25×10^{-5}	1

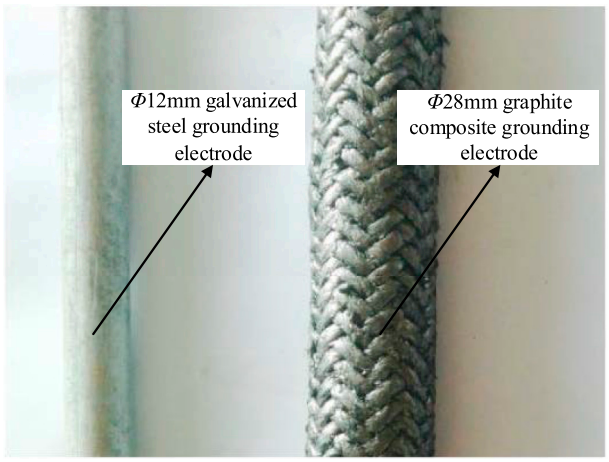

FIGURE 7 | Physical picture of the grounding electrode.

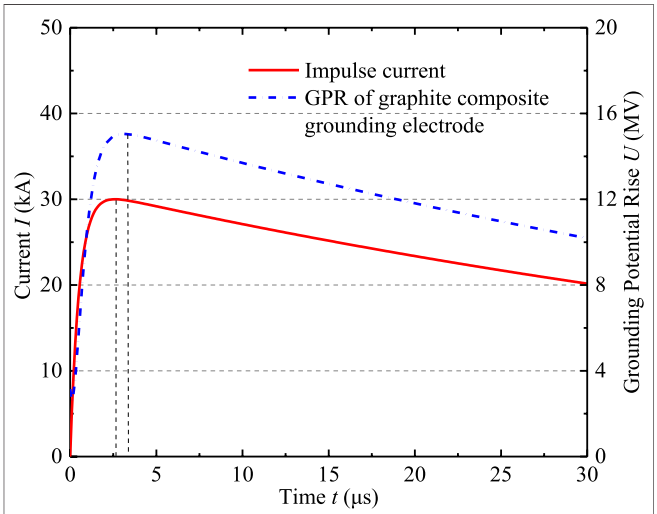

FIGURE 8 | Waveform of grounding potential rise when capacitance effect is dominant.

coefficient, which is equal to the ratio of impulse grounding impedance R_{ch} to power frequency grounding resistance R_g. It can be seen that the calculated results are in good agreement with the experiment results of Wen *et al* (Yang et al., 2022). In general, the proposed simulation models and algorithms are correct, and the results are credible.

EFFECT OF VARIOUS PHYSICAL EFFECTS ON IMPULSE CHARACTERISTICS OF GRAPHITE COMPOSITE GROUNDING ELECTRODES

Under the action of high frequency lightning current and fault current, the grounding grid presents impedance characteristics, including resistance component and reactance component. Therefore, in order to analyze the grounding characteristics of graphite composite grounding materials, the grounding impedance characteristics should be analyzed under the action of alternating current. The physical processes affecting the grounding impedance include skin effect, inductance effect, capacitance effect and spark discharge effect. In this paper, the influence of four physical effects on graphite composite grounding materials is analyzed and calculated. The results are compared with traditional metal grounding materials (galvanized steel). The physical picture and measured parameters of grounding electrode of two materials are shown in **Figure 7** and **Table 2**.

In the simulation, the length of grounding electrode is 10, 30, 60 m, the buried depth is 0.8m, the critical breakdown field strength of soil is 400 kV/m, the lightning current parameter is 2.6/50 μs, and the amplitude is 30 kA. In **Table 2**, Φ is the diameter of grounding electrode; δ is the grounding material resistivity, Ω·m; ε_r is the relative permeability of grounding material.

Capacitance Effect

When only capacitance effect is considered, inductance effect, skin effect and spark discharge effect should be ignored. That is, in the simulation calculation process, the grounding electrode inductance, high frequency resistance and iterative algorithm are not involved in the simulation calculation. The α_C is defined as the impulse coefficient of different soil resistivity. It is found that the impulse coefficients α_C of both materials are less than the value 1, and the maximum error between α_C and value 1 is not more than 0.6%. It shows that capacitance effect can reduce impulse grounding impedance under the impulse current, but the effect is very small.

The capacitance effect will not only reduce the impulse grounding impedance, but also cause the grounding potential rise waveform on the grounding electrode lagging behind the impulse current waveform. **Figure 8** shows the impulse current waveform and grounding potential rise waveform of graphite composite grounding electrode with soil resistivity ρ of 4,000 Ω m and length l of 10 m.

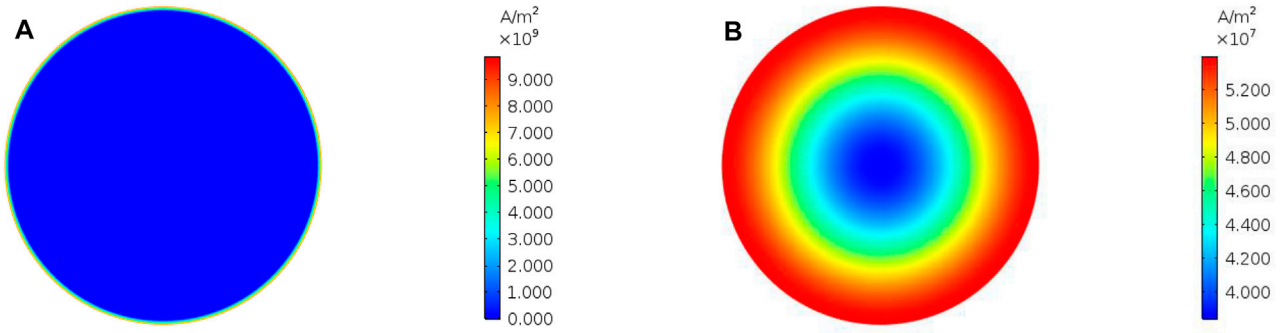

FIGURE 9 | Skin effect of grounding electrodes. **(A)** Current density of Φ12 mm galvanized steel grounding electrode cross section. **(B)** Current density of Φ28 mm graphite composite grounding electrode cross section.

Skin Effect

Finite element numerical calculation method is used to compare and analyze the skin effect of grounding electrodes of different materials in the flow of high frequency current. Galvanized steel grounding electrode of diameter Φ = 12 mm and graphite composite grounding electrode of diameter Φ = 28 mm are applied during simulation according to practical grounding engineering. The current frequency is 100 kHz, and the length l of grounding electrode is 1 m. The simulation results are shown in **Figure 9**.

It can be seen that the current density distribution of galvanized steel grounding electrode is extremely uneven due to skin effect, and the current is mostly concentrated on the external surface of the grounding electrode. This results in a significant reduction in the actual area of current flowing through the grounding electrode. On the contrary, the current density distribution of graphite composite grounding electrode is relatively uniform.

Due to the influence of high frequency current, the cross-sectional area of the actual current flowing through the grounding electrode decreases, thereby increasing the resistance of the grounding electrode. In order to compare and analyze the influence of skin effect on the grounding characteristics of two grounding materials, the resistance R of grounding electrode under different frequencies is used as the influencing factor of skin effect, which can be calculated according to **Eq. 11**.

$$R = \begin{cases} \dfrac{l}{\pi\sigma r^2}, & \delta \geq r \\ \dfrac{l}{\pi\sigma\delta(2r-\delta)}, & \delta < r \end{cases} \tag{11}$$

where σ is the conductivity of the conductor; δ is the radial depth that the current flowing through the grounding electrode can reach due to the skin effect, and is calculated by **Eq. 12**.

$$\delta = \sqrt{\frac{2}{\omega\mu_r\mu_0\sigma}} \tag{12}$$

where μ_0 is vacuum permeability; μ_r the relative permeability of grounding material. The actual lightning current frequency is mostly concentrated in 0–200 kHz. The resistance R of graphite composite grounding electrode and galvanized steel grounding electrode in the unit length can be obtained by calculation. As shown in **Figure 10**, as the frequency increases, the resistance R of galvanized steel grounding electrode increases greatly. In contrast, the increase in resistance of graphite composite grounding electrode is small, which indicates that the graphite composite grounding electrode has less affected by the skin effect under the action of high frequency current.

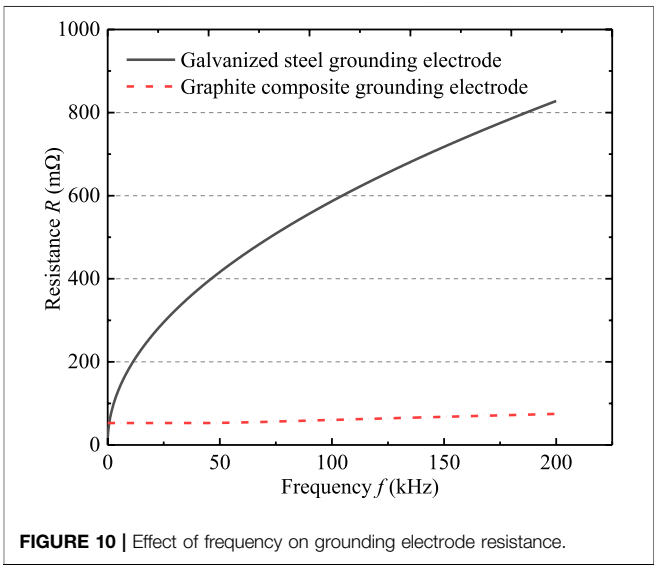

FIGURE 10 | Effect of frequency on grounding electrode resistance.

Considering the capacitance effect, the impulse coefficient α_{sc} and α_c of the grounding electrode at different materials are calculated with and without the skin effect. In order to facilitate the analysis of the influence of skin effect on the grounding electrode impulse characteristics, the influence rate η_s of skin effect on the impulse coefficient is defined. The effect of skin effect on the impulse characteristics of grounding electrode can be solved by **Eq. 13**.

$$\eta_s = (\alpha_{SC} - \alpha_C) \times 100\% \tag{13}$$

TABLE 3 | Influence rate η_s of skin effect (%).

Soil resistivity ρ (Ω·m)	Galvanized steel grounding electrode			Graphite composite grounding electrode		
	10 m	30 m	60 m	10 m	30 m	60 m
50	7.07	42.91	90.68	0.05	0.36	0.92
200	1.81	14.09	41.65	0.01	0.11	0.34
500	0.73	5.88	20.12	0.01	0.04	0.16
1,000	0.35	2.93	10.54	0	0.02	0.06
2000	0.18	1.43	5.22	0	0.01	0.06
4,000	0.02	0.56	2.44	0	0	0.01

The effect rate of skin effect on the grounding electrodes is shown in **Table 3**. It can be seen that the change of impulse coefficient of galvanized steel grounding electrode is greater than that of graphite composite grounding electrode affected by lightning current. The influence of graphite composite grounding electrode is less than 1%.

On the whole, the resistance R of the grounding electrode is related to its length l, and the longer the length l, the larger the resistance R. Therefore, when the length of the grounding electrode is long, the skin effect has a great influence. In high soil resistance area, the lightning grounding current flows through the grounding electrode, and the current flowing to the surrounding soil is small, resulting in large impulse grounding impedance. At this time, the proportion of GPR of grounding electrode in the total GPR is small, so the skin effect is weak.

Inductance Effect

In order to fully consider the influence of the inductance effect, this paper divides the inductance of the grounding electrode into self-inductance and mutual inductance, and the mutual inductance can be obtained by the Neumann equation (Ma et al., 2015). Since the magnetic flux generated by the current through the conductor is respectively closed inside and outside the conductor, the self-inductance is equal to the sum of external self-inductance and inner self-inductance. The external self-inductance L_e can ignore the influence of frequency and it is calculated by **Eq. 14**.

$$L_e = \frac{\mu_0 l}{2\pi}\left(\ln\frac{2l}{r} - 1\right) \tag{14}$$

where μ_0 is vacuum permeability; l is the length of grounding electrode; r is the radius of the grounding electrode. The internal self-inductance L_i is calculated by the low frequency current, as shown in **Eq. 15**.

$$L_i = \frac{\mu_r \mu_0 l}{8\pi} \tag{15}$$

where μ_0 is vacuum permeability; μ_r the relative permeability of grounding material; l is the length of grounding electrode. When the current frequency is high, the internal self-inductance of grounding electrode changes due to skin effect, and is solved according to **Eq. 16**.

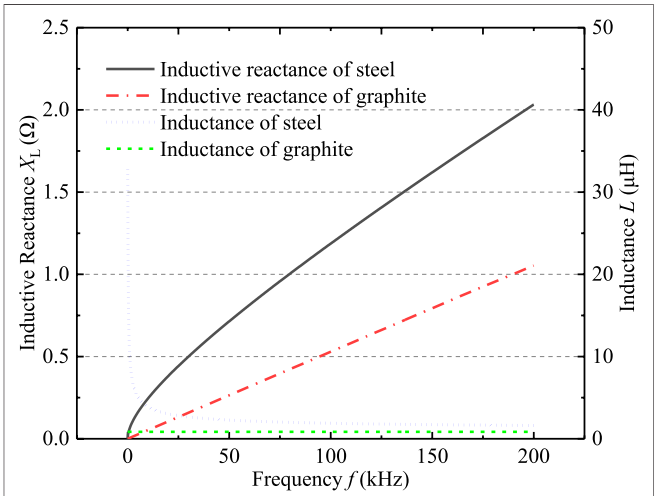

FIGURE 11 | Effect of frequency on the inductance of the grounding electrode.

$$L_i = \frac{l}{2\pi r}\sqrt{\frac{\mu_r \mu_0}{2\omega\sigma}} \tag{16}$$

where μ_0 is vacuum permeability; μ_r the relative permeability of grounding material; l is the length of grounding electrode; r is the radius of the grounding electrode; σ is the conductivity of the grounding electrode. As the sinusoidal alternating current at different frequencies changes, the self-inductance and inductive reactance per unit length of graphite composite grounding electrode and galvanized steel grounding electrode are shown in **Figure 11**.

Under the influence of 0–200 kHz AC current, the inductive reactance of graphite composite grounding electrode is smaller than that of galvanized steel grounding electrode. This is because the galvanized steel grounding electrode is the paramagnetic material, and its magnetic permeability is much larger than that of the graphite composite grounding electrode, resulting in a larger inductance of galvanized steel grounding electrode.

Considering the capacitance effect, skin effect and inductance effect simultaneously, the impulse coefficient α_{SLC} of grounding electrode is calculated, and the influence rate η_L of inductance effect is obtained by **Eq. 17**.

$$\eta_L = (\alpha_{SLC} - \alpha_{SC}) \times 100\% \tag{17}$$

TABLE 4 | Influence rate η_L of inductance effect (%).

Soil resistivity ρ (Ω·m)	Galvanized steel grounding electrode			Graphite composite grounding electrode		
	10 m	30 m	60 m	10 m	30 m	60 m
50	22.83	117.88	194.07	12.51	107.19	164.29
200	1.69	55.6	126.42	0.12	44.53	114.74
500	0.43	18.49	78.21	0.1	8.17	67.76
1,000	0.26	3.56	46.05	0.05	0.22	35.89
2000	0.18	1.02	17.22	0.02	0.08	8
4,000	0.1	0.38	1.88	0.01	0.02	0.13

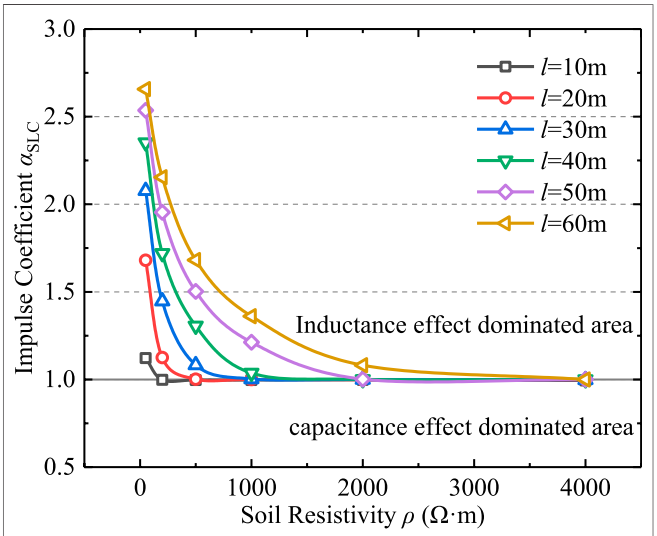

FIGURE 12 | Impulse coefficient of graphite composite grounding electrode without spark discharge effect.

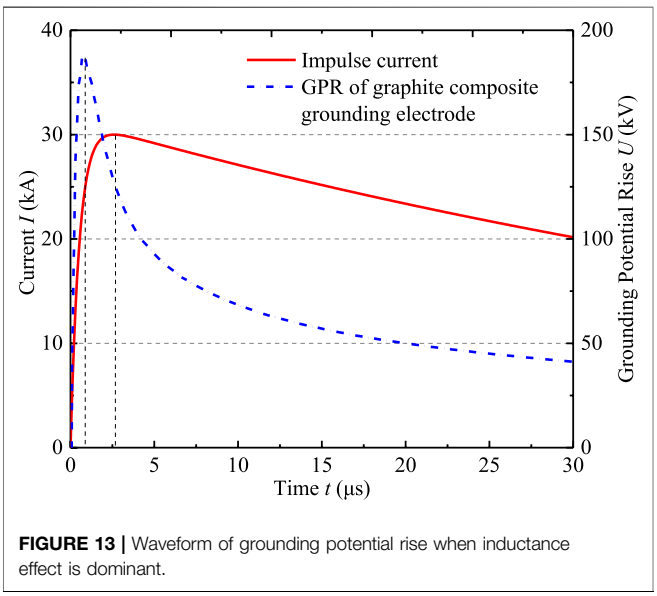

FIGURE 13 | Waveform of grounding potential rise when inductance effect is dominant.

As shown in **Table 4**, the galvanized steel grounding electrode is more affected than graphite composite grounding electrode due to the inductance effect. Overall, the longer the length l of grounding electrode, the stronger the inductance effect, and the greater the obstruction of current flowing to the far position of grounding electrode. With the increase of soil resistivity, the proportion of GPR generated by the inductance of grounding electrode in total GPR decreases. Therefore, the inductance effect of grounding electrode has little effect on its impulse grounding characteristics in the areas with high soil resistivity.

Without considering the spark discharge effect, the variation of impulse coefficient of calculated graphite composite grounding electrode with soil resistivity is shown in **Figure 12**. In most cases, the impulse coefficient α_{SLC} is greater than the value 1. As skin effect has little effect on graphite composite grounding material, it is mainly caused by the inductive effect of grounding electrode. **Figure 13** shows the impulse response curve when the soil resistivity ρ is 50 Ω m and the grounding electrode length l is 60 m. It can be seen that the grounding impedance of grounding electrode presents inductance characteristics, and the GPR waveform is ahead of the impulse current. When the grounding electrode is short or the soil resistivity is high, the impulse coefficient α_{SLC} appears to be less than the value 1. This is because the conductivity of soil is poor, and the influence of inductance effect and skin effect are small. At this time, the grounding capacitance of grounding electrode is involved in the diffusion of high frequency current, resulting in significant capacitance characteristic of impulse grounding impedance, and the impulse grounding impedance is less than power frequency grounding resistance.

Spark Discharge Effect

Under the effect of the impulse current, when the electric field intensity E of the soil around the grounding electrode reaches the critical breakdown electric field intensity E_c of the soil, the soil ionization occurs due to the breakdown. The soil resistivity around the grounding electrode is greatly reduced. An iterative algorithm of equivalent radius of grounding electrode is used to simulate the spark discharge process and calculate the impact grounding impedance of grounding electrode. The influence rate η_D of spark discharge effect is calculated by **Eq. 18**, as shown in **Table 5** and **Table 6**.

$$\eta_D = (\alpha - \alpha_{SC}) \times 100\% \tag{18}$$

TABLE 5 | Influence rate η_D of spark discharge effect (%).

Soil resistivity ρ (Ω·m)	Galvanized steel grounding electrode			Graphite composite grounding electrode		
	10 m	30 m	60 m	10 m	30 m	60 m
50	−33.22	−56.54	−76.1	−19.8	−28.63	−33.33
200	−51.42	−50.36	−75.16	−47.51	−33.37	−45.94
500	−64.68	−43.97	−66.04	−60.51	−31.82	−46.03
1,000	−72.04	−48.11	−58.40	−68.64	−43.44	−44.28
2000	−77.95	−61.24	−50.08	−75.32	−60.52	−40.17
4,000	−82.42	−71.89	−53.09	−79.8	−67.98	−51.8

TABLE 6 | Impulse grounding impedance R_{ch} of different material grounding electrodes (Ω).

Soil resistivity ρ (Ω·m)	Galvanized steel grounding electrode			Graphite composite grounding electrode		
	10 m	30 m	60 m	10 m	30 m	60 m
50	6.77	6.2	5.95	5.96	5.56	5.45
200	14.48	13.9	13.12	13.26	12.32	11.79
500	25.26	23.22	21.82	24.77	20.6	19.53
1,000	39.4	33.6	32.05	39.25	30.34	28.48
2,000	61.35	47.28	46.96	61.58	41.92	41.47
4,000	95.44	66.23	66.01	99.23	67.53	58.34

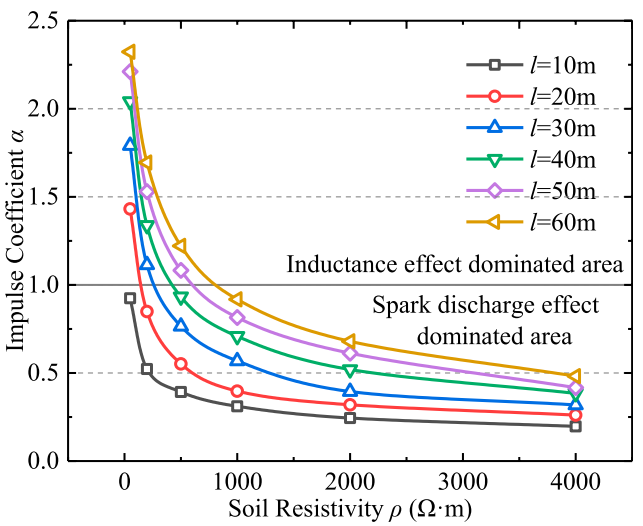

FIGURE 14 | Curve of impulse coefficient of graphite composite grounding electrode.

Where the impulse coefficient α_{SLC} considering capacitance effect, skin effect and inductance effect; the impulse coefficient α considering capacitance effect, skin effect, inductance effect and spark discharge. The spark discharge effect of galvanized steel grounding electrode is slightly better than that of graphite composite grounding electrode, but graphite composite grounding electrode is less affected by inductance effect and skin effect, so it has better current flowing capability. Comparing the impulse grounding impedance, the inductance effect is less affected when the soil resistivity is high and the grounding electrode length is short, and the galvanized steel grounding electrode is greatly affected by the spark discharge effect, resulting in its impulse grounding impedance R_{ch} is smaller than graphite. But as a whole, the impulse grounding impedance of graphite composite grounding electrode is mostly smaller than that of steel. In the actual engineering design of tower grounding engineering, large-size square grounding electrodes with elongated conductors are usually used. The grounding electrode is more affected by inductance effect and skin effect. Therefore, the impulse grounding characteristic of graphite composite grounding electrode is better than that of galvanized steel grounding electrode.

In summary, the inductance effect and skin effect will increase the grounding impedance of the grounding electrode. Conversely, the capacitance effect and sparking discharge effect can reduce the impulse grounding impedance. For graphite composite grounding electrode, the capacitance effect and skin effect have little effect, so this paper only analyzes the influence of inductance effect and spark discharge effect. It can be seen from **Figure 14** that in the low soil resistivity area and the grounding electrode is long, the grounding electrode impulse coefficient α is greater than the value 1. The GPR generated by inductance effect accounts for a large proportion of the total GPR, leading to the inductance effect being dominant. However, as the soil resistivity ρ increases, the impulse coefficient α decreases and the spark discharge effect increases. When α is less than the value 1, the spark discharge effect is more dominant than inductance effect.

OPTIMIZATION OF LENGTH OF FLEXIBLE GRAPHITE COMPOSITE GROUNDING ELECTRODE

In practical engineering applications, in order to improve the current dispersion characteristics of tower grounding grid, the effect of inductance effect should be minimized or the effect of spark discharge effect should be increased to make the spark discharge effect of grounding electrode dominant. According to

TABLE 7 | Computation parameters of lightning current impulse waveform.

Waveform parameter	Front time T_1 (μs)	Time to half value T_2 (μs)	Peak value I_m (kA)
Waveform 1	0.8	48	12
Waveform 2	2.6	50	30
Waveform 3	8	69	30

TABLE 8 | Soil resistivity critical value on which dominant inductance effect switch to spark discharge effect.

Waveform parameter	Critical value of soil resistivity ρ_c (Ω·m)					
	10 m	20 m	30 m	40 m	50 m	60 m
Waveform 1	144	455	824	1,237	1,638	2039
Waveform 2	41	138	263	428	624	824
Waveform 3	12	53	97	164	238	318

TABLE 9 | Critical value of normalized parameters on which dominant inductance effect switch to dominant spark discharge effect.

Waveform parameter	Normalized parameters S (kA·Ω)					
	10 m	20 m	30 m	40 m	50 m	60 m
Waveform 1	173	273	330	371	393	408
Waveform 2	122	207	263	321	374	412
Waveform 3	35	80	97	123	143	159

the field measurement results of lightning current, this paper selects three kinds of the most common lightning current, the waveforms are shown in **Table 7**.

Waveform 1 is a typical initial waveform of lightning impulse current, which is mainly used to simulate the significant inductance effect. Waveform 2 is the standard lightning current waveform recommended for lightning protection calculation. Waveform 3 is a typical secondary waveform of lightning impulse current, which is mainly used to simulate the significant spark discharge effect.

The impulse coefficient α of graphite composite grounding electrode is calculated under different lightning current waveforms.

According to the fitting of the result curve, the soil resistivity critical value ρ_c was estimated, which is the soil resistivity when the pulse characteristic is converted from the dominance of inductance effect to the dominance of spark discharge effect. As shown in **Table 8**, the inductance effect dominates when the soil resistivity is less than the corresponding critical value, otherwise the spark discharge effect dominates.

In order to facilitate the optimal design of grounding electrode, it is necessary to make a general quantitative description of the dominant range of inductance effect and spark effect. Therefore, the normalization parameter S is defined as the quantitative criterion of conversion, which can be calculated by **Eq. 19**.

$$S = \frac{\rho_C I_m}{l} \tag{19}$$

According to **Table 9**, when the soil resistivity ρ and the lightning impulse current front waveform time T_1 and the peak value I_m are known, the appropriate grounding electrode length l can be selected to ensure that the impulse characteristics are always dominated by spark discharge effect, so as to reduce the impulse impedance. For example, when the soil resistivity ρ is 500 Ω m and the lightning current is waveform 2, the grounding electrode length l is selected as 40 m, and the corresponding normalized parameter S is 375 kA Ω, which is larger than the 321 kA Ω in **Table 9**. The spark discharge effect dominates, and the impulse grounding impedance R_{ch} is smaller than the power frequency grounding resistance R_g. Meanwhile, in order to facilitate engineers to conservatively estimate the impulse characteristics of graphite composite grounding electrode, the maximum value of 412 kA Ω in **Table 9** is taken as the critical value of normalized parameter for converting inductance effect into spark discharge effect. It should be pointed out that the above conclusion is determined according to the soil critical breakdown field strength E_c of 400 kV/m, which has a certain deviation from the actual E_c value. When E_c>400 kV/m, the corresponding normalized parameter S is larger than the values listed in **Table 9**, and when E_c<400 kV/m, S is smaller than the values in **Table 9**.

CONCLUSION

This paper presents a frequency domain electrical network analysis method to simulate the impulse characteristics of grounding electrodes. The impulse characteristics of typical metal grounding electrode and graphite composite grounding electrode are calculated, and the following conclusions are obtained.

1) Compared with the galvanized steel grounding electrode, the graphite composite grounding electrode has little effect on skin effect and inductance effect, and the graphite composite grounding electrode has better current dispersion ability under the impulse current.
2) The inductance effect and skin effect can increase the grounding impedance of grounding electrode, while the capacitance effect and spark discharge effect can reduce it. However, the capacitance effect is very small compared with the spark discharge effect, which can be ignored.
3) The longer the grounding electrode length, the more obvious the effect of inductance and skin effect. However, with the increase of soil resistivity, the influence of the two decreases, and the spark discharge effect increases and gradually dominates.
4) The normalized parameter S is defined to quantitatively distinguish the influence range of inductance effect and

spark discharge effect. The length of graphite composite grounding electrode can be optimized by critical value *S*, so as to ensure that the impulse characteristics are always dominated by spark effect, and finally the purpose of reducing impulse grounding impedance is achieved. To conservatively estimate the impulse characteristics of grounding electrode, the recommended *S* value is 412 kA Ω as the critical value to convert inductive effect into spark discharge effect (Shen and Raksincharoensak, 2021b).

DATA AVAILABILITY STATEMENT

The original contributions presented in the study are included in the article/Supplementary Material, further inquiries can be directed to the corresponding author.

AUTHOR CONTRIBUTIONS

YH: conceptualization, writing-original draft preparation, software; TH: software; YA: funding acquisition, validation; JF: Simulation and figures; MC: project administration; HX: supervision; WS: supervision; CD: validation.

FUNDING

This manuscript was supported in part by the Natural Science Foundation of China under Grant 51807113, in part by the Natural Science Foundation of Shandong Province under Grant ZR202103040796 and the Natural Science Foundation of Jiangsu Province under Grant SBK2020042717.

REFERENCES

de Lima, A. C. S., and Portela, C. (2007). Inclusion of Frequency-dependent Soil Parameters in Transmission-Line Modeling. *IEEE Trans. Power Deliv.* 22 (1), 492–499. doi:10.1109/tpwrd.2006.881582

Deng, C., Yang, Y., Tong, X., Dong, X., and Peng, Q. (2012). Impulse Characteristics Analysis of Grounding Devices. *High Voltage Eng.* 38 (9), 1–8. doi:10.3969/j.issn.1003-6520.2012.09.044

Deng, C., Yang, Y., Dong, X., Ma, S., Peng, Q., and Wang, X. (2013). Development of Impulse High Current Testing System of Grounding Devices and Testing of tower Grounding Impulse Characteristics. *High Voltage Eng.* 39 (6), 1527–1535. doi:10.3969/j.issn.1003-6520.2013.06.035

Feng, Z., Wen, X., Tong, X., Lu, H., Lan, L., and Xing, P. (2015). Impulse Characteristics of Tower Grounding Devices Considering Soil Ionization by the Time-Domain Difference Method. *IEEE Trans. Power Deliv.* 30 (4), 1906–1913. doi:10.1109/tpwrd.2015.2425419

Gazzana, D. S., Bretas, A. S., Dias, G. A. D., Telló, M., Thomas, D. W. P., and Christopoulos, C. (2014). The Transmission Line Modeling Method to Represent the Soil Ionization Phenomenon in Grounding Systems. *IEEE Trans. Magn.* 50 (2), 103–107. doi:10.1109/tmag.2013.2283714

Gong, R., Ruan, J., Hu, Y., Wu, Y., and Jin, S. (2016). "Research on Flexible Graphite-Copper Composited Electrical Grounding Material," in Proceeding of the 12th IET International Conference on AC and DC Power Transmission (ACDC 2016), Beijing, China (IEEE), 1–6. doi:10.1049/cp.2016.0403

Grcev, L. (2009). Time- and Frequency-dependent Lightning Surge Characteristics of Grounding Electrodes. *IEEE Trans. Power Deliv.* 24 (4), 2186–2196. doi:10.1109/tpwrd.2009.2027511

Grcev, L. (2009). Impulse Efficiency of Ground Electrodes. *IEEE Trans. Power Deliv.* 24 (1), 441–451. doi:10.1109/tpwrd.2008.923396

He, J., Zeng, R., Tu, Y., Zou, J., Guan, S., and Guan, Z. (2003). Laboratory Investigation of Impulse Characteristics of Transmission tower Grounding Devices. *IEEE Trans. Power Deliv.* 18 (3), 994–1001. doi:10.1109/tpwrd.2003.813802

He, J., and Zhang, B. (2015). Progress in Lightning Impulse Characteristics of Grounding Electrodes with Soil Ionization. *IEEE Trans. Ind. Applicat.* 51 (6), 4924–4933. doi:10.1109/tia.2015.2427124

Hu, Y., An, Y., Xian, R., Li, H., Ruan, J., Huang, D., et al. (2016). "Study on Magnetic Properties of Flexible Graphite Composite Grounding Material," in Proceeding of the 2016 IEEE International Conference on High Voltage Engineering and Application, Chengdu, China, Sept. 2016 (IEEE), 1–4. doi:10.1109/ICHVE.2016.7800753

Hu, Y., Ruan, J., Gong, R., Liu, Z., Wu, Y., and Wen, W. (2014). Flexible Graphite Composite Electrical Grounding Material and its Application in tower Grounding Grid of Power Transmission System. *Power Syst. Technol.* 38 (10), 2851–2857. doi:10.13335/j.1000-3673.pst.2014.10.037

Huang, D., Xia, J., Ruan, J., Wu, Y., and Quan, W. (2019). Characteristics of the Flexible Graphite Grounding Material and its Engineering Application. *IEEE Access* 7, 59780–59787. doi:10.1109/access.2019.2913558

Lorentzou, M. I., Hatziargyriou, N. D., and Papadias, B. C. (2003). Time Domain Analysis of Grounding Electrodes Impulse Response. *IEEE Trans. Power Deliv.* 18 (2), 517–524. doi:10.1109/tpwrd.2003.809686

Ma, Z., Zhou, X., Shang, Y., and Zhou, L. (2015). Form and Development Trend of Future Distribution System. *Proc. CSEE* 35 (6), 1289–1298. doi:10.13334/j.0258-8013.pcsee.2015.06.001

Mentre, F. E., and Grcev, L. (1994). EMTP-based Model for Grounding System Analysis. *IEEE Trans. Power Deliv.* 9 (4), 1838–1849. doi:10.1109/61.329517

Mousa, A. M. (1994). The Soil Ionization Gradient Associated with Discharge of High Currents into Concentrated Electrodes. *IEEE Trans. Power Deliv.* 9 (3), 1669–1677. doi:10.1109/61.311195

Nekhoul, B., Labie, P., Zgainski, F. X., Meunier, G., Morillon, F., and Bourg, S. (1996). Calculating the Impedance of a Grounding System. *IEEE Trans. Magn.* 32 (3), 1509–1512. doi:10.1109/20.497536

Shen, X., Ouyang, T., Khajorntraidet, C., Li, Y., Li, S., and Zhuang, J. (2022). Mixture Density Networks-Based Knock Simulator. *Ieee/asme Trans. Mechatron.* 27, 159–168. doi:10.1109/TMECH.2021.3059775

Shen, X., and Raksincharoensak, P. (2021a). Pedestrian-aware Statistical Risk Assessment. *IEEE Trans. Intell. Transport. Syst.*, 1–9. doi:10.1109/TITS.2021.3074522

Shen, X., and Raksincharoensak, P. (2021b). Statistical Models of Near-Accident Event and Pedestrian Behavior at Non-signalized Intersections. *J. Appl. Stat.*, 1–21. doi:10.1080/02664763.2021.1962263

Tao, S., Zhang, X., Wang, Y., and Yang, J. (2018). Transient Behavior Analysis of Offshore Wind Turbines during Lightning Strike to Multi-Blade. *IEEE Access* 6, 22070–22083. doi:10.1109/access.2018.2828043

Visacro, S., and Rosado, G. (2009). Response of Grounding Electrodes to Impulsive Currents: An Experimental Evaluation. *IEEE Trans. Electromagn. Compat.* 51 (1), 161–164. doi:10.1109/temc.2008.2008396

Wen, X., Feng, Z., Lu, H., Tong, X., Lan, L., Chen, W., et al. (2016). Sparkover Observation and Analysis of the Soil under the Impulse Current. *IET Sci. Meas. Tech.* 10 (3), 228–233. doi:10.1049/iet-smt.2015.0082

Xiao, W., Hu, Y., Ruan, J., Zhan, Q., and Huang, D. (2017). Flexible Graphite Composite Electrical Grounding Material and its Grounding Application Features. *Power Syst. Technol.* 32 (2), 85–94. doi:10.19595/j.cnki.1000-6753.tces.2017.02.010

Yang, N., Yang, C., Xing, C., Ye, D., Jia, J., Chen, D., et al. (2021). Deep Learning-based SCUC Decision-making: An Intelligent Data-driven Approach with Self-learning Capabilities. *IET Generation Trans. Dist* 16, 629–640. doi:10.1049/gtd2.12315

Yang, N., Yang, C., Wu, L., Shen, X., Jia, J., Li, Z., et al. (2022). Intelligent Data-Driven Decision-Making Method for DynamicMultisequence: An

E-Seq2Seq-Based SCUC Expert System. *IEEE Trans. Ind. Inf.* 18, 3126–3137. doi:10.1109/TII.2021.3107406

Zhang, X. (2018). Computation of Lightning Transients in Large Scale Multiconductor Systems. *IEEE Access* 6, 76573–76585. doi:10.1109/access.2018.2883385

Conflict of Interest: TH, MC, HX, WS and CD are employed by Construction Branch of State Grid Jiangsu Electric Power Co., Ltd.

The remaining authors declare that the research was conducted in the absence of any commercial or financial relationships that could be construed as a potential conflict of interest.

Publisher's Note: All claims expressed in this article are solely those of the authors and do not necessarily represent those of their affiliated organizations, or those of the publisher, the editors and the reviewers. Any product that may be evaluated in this article, or claim that may be made by its manufacturer, is not guaranteed or endorsed by the publisher.